Selective ion sensing in aqueous media with ESIPT active fluorescent probes – A particular case for hypochlorite detection

Christian Julio Murga Cotrina, Arghyadeep Bhattacharyya, Shenming Wang, Baptiste Amouroux, Nicolas Casaretto, Sophie Bourcier, Isabelle Leray, Gaël Zucchi

Selective Ion Sensing in Aqueous Media with ESIPT Active Fluorescent Probes – A Particular Case for Hypochlorite Detection

Christian Julio Murga Cotrina,[a] Arghyadeep Bhattacharyya,[a,b] Shenming Wang,[a] Baptiste Amouroux,[c] Nicolas Casaretto,[d] Sophie Bourcier, [d] Isabelle Leray,[c] and Gaël Zucchi [a,*]

[a] Laboratoire de Physique des Interfaces et des Couches Minces, CNRS, Ecole Polytechnique, Institut Polytechnique de Paris, 91128 Palaiseau, France.

[b] Present address: Department of Physical Chemistry, Environmental Sciences and Biochemistry and INAMOL, University of Castilla-La Mancha (UCLM), Avenida Carlos III, S / N, 45071 Toledo, Spain.

[c] Université Paris-Saclay, ENS Paris-Saclay, CNRS, Photophysique et Photochimie Supramoléculaires et Macromoléculaires, 91190, Gif-sur-Yvette, France.

[d] Laboratoire de Chimie Moléculaire, CNRS, Ecole polytechnique, Institut Polytechnique de Paris, 91128 Palaiseau, France.

Email: gael.zucchi@polytechnique.edu

Abstract: We report two ESIPT active novel fluorescent probes, **1** and **2**, based on benzoxazole and benzimidazole units, respectively. Their sensing aptitude towards metal ions in aqueous media is reported. A specific response of **1** to Al^{3+} and, to a lesser extent, Zn^{2+}, was found, while the emission of **2** is highly impacted by the Al^{3+}, Cu^{2+}, Fe^{2+} and Fe^{3+} metal ions by either a blue shift or a quenching of the emission. Emission of **2** also shows a relative sensitivity to the Ni^{2+} and Hg^{2+} cations. Anions sensing studies on **2** revealed a unique emission in presence of hypochlorite ions, while glyphosate and

aminomethylphosphonic acid have the effect to decrease the emission intensity by 40% and 75%, respectively. Investigations on the recognition mechanism led to the conclusion that Al^{3+} was inhibiting the ESIPT process by deprotonation of the phenol group, and that a fast but weak interaction was taking place between the hypochlorite ion and **2**.

1. Introduction

Chemical analysis of water, and in particular drinking water, is of tremendous importance for obvious sanitary reasons. The importance of detecting metal ions dissolved in water is due to the adverse effects they exert on the human body and the environment. The very broad range of applications using aluminum makes it one of the most widely used metals [1-4]. Al^{3+} is prevalent in the environment due to acid rain and the use of aluminum in utensils, industries, or aircraft. In consequence, Al^{3+} is found in the food chain and particularly in animals, plant tissues and natural water [5-7]. In a concentrated form, it causes widespread damage to flora and fauna [8-10]. Accumulation of Al^{3+} in the human body results in deadly Parkinson and Alzheimer diseases, and neurofibrillary, enzymatic and neurotransmitory disorders [11-13]. World Health Organization (WHO) has set the threshold amount of Al^{3+} to be 200 μg/L (7.41 μM) [14]. This highlights the importance of detecting Al^{3+} in the environment, and especially in water. Zinc, after iron, is the second most abundant metal ion in the body where it plays a vital role, but, upon accumulation, it shows cytotoxic effects [15-17]. On the other hand, Zn^{2+} is a major contaminant in food and agricultural wastes [18].

In the view of preserving human health, a common way to eliminate pathogens from water and avoid invasion of microorganisms is the use of bleach, a solution of sodium hypochlorite. However, the concentration of hypochlorite in water should be controlled as it can be hazardous for human body and lead to the development of diseases because

of the formation of chlorination by-products [19] that are also toxic for the environment [20].

To detect ions in solution, the commonly employed techniques are flame atomic absorption spectrometry, acid-base titrimetry using glass pH electrode, induced plasma-atomic emission spectrometry and differential pulse stripping anodic voltammetry [21-24]. However, most of them require sophisticated instrumentation, sample preparation and pre-treatment restricting the ease of detecting species in solution. Then, spectrofluorometric methods stand out due to potentially high sensitivity and specificity with rapid monitoring, non-destruction of the sample, quick response and non-requirement of a heavy and expensive instrumentation [25].

Excited State Intramolecular Proton transfer (ESIPT) has been recently used owing to the ratiometric nature of detection, high stokes shift and bright luminescence upon binding to metal ions [26-28]. In a ratiometric detector, the emission of at least two bands is impacted by an interaction with the analyte, giving rise to an internal referencing and with enhanced sensitivity [25]. Moreover, ESIPT active fluorescent probes show a particular affinity for ions like Zn^{2+}, Cd^{2+} and Al^{3+}, most probably due to the ligand cavity being ideally compatible with the ionic radii of these cations. However, the principal bottleneck is the detection being achieved in aqueous or mixed organic/aqueous media [27]. Chen *et al.* have recently reported a benzoxazole-based fluorescent probe for the detection of Zn^{2+} in water [30]. Similarly, Yue *et al.* reported a naphthalene-based platform to detect Al^{3+} in pure water [31] but the response was a 'turn on' response instead of a ratiometric one. A rare (hydroxyphenyl)benzothiazole derivative described to be an effective HClO/ClO^- ESIPT probe was reported some time ago [32].

We hereby describe the synthesis and sensing aptitude through ESIPT of a benzoxazole derivative, 2-(2-hydroxy-3-hydroxymethyl-5-methoxyphenyl)-benzoxazole (**1**), and that

of a benzimidazole one, 2-(2-hydroxy-3-hydroxyiminomethyl-5-methylphenyl)-benzimidazole (**2**). We report how their design can lead to fluorometric probes showing a particular sensitivity to Al^{3+}, Zn^{2+}, and ClO^- ions. In the quest of a better understanding of this sensitivity, the possible probe/analyte interactions are also discussed.

2. Experimental

2.1. General information

All chemicals were purchased from Sigma Aldrich and used without further purification. Spectroscopic grade solvents were used throughout the spectroscopic experiments. Compounds I1-I5 have already been reported [30, 33, 34].

NMR spectra were recorded on a Bruker Advance 300 spectrometer. High-resolution mass spectrometry (HR-MS) experiments were performed on Tims-TOF mass spectrometer (Bruker, France). Absorption spectra were recorded with an Agilent Technologies Cary 60 UV–Vis spectrophotometer, and emission spectra were obtained using a HORIBA Jobin Yvon spectrofluorimeter Model Fluoromax-4. Details on sample preparation and measurements can be found in the Supplementary Material.

Quantum yields were measured as described previously [35]. The values were reported as an average of three independent determinations and the error is within 10%.

2.2. Synthetic procedures

2-(2-hydroxy-3-hydroxymethyl-5-methoxyphenyl)-benzoxazole (1). A suspension of **I3** (270 mg, 1 mmol) and $NaBH_4$ (152 mg, 4 mmol) in 10 mL of methanol was stirred for 5 h at room temperature followed by evaporation of methanol using a rotary evaporator. The residue was washed with 10 mL of distilled water and 37% HCl was added until neutral pH was obtained. A white precipitate immediately formed which was filtered and

washed thoroughly with water and dried under vacuum. Yield: 211 mg (78%). ^{1}H-NMR ($CDCl_3$, 400 MHz): δ (ppm) 7.75 (1H, m), 7.64 (H, m), 7.47 (1H, d, J = 3.02 Hz, H7), 7.42 (2H, m, H4 and H5), 7.12 (1H, d, J = 3.02 Hz, H8), 4.82 (2H, s, H12), 3.89 (3H, s, H10). ^{13}C-NMR ($CDCl_3$, 100 MHz): δ (ppm) 152.36, 151.02, 149.09, 130.28, 125.52, 125.12, 120.21, 119.28, 110.70, 110.03, 108.96, 61.86, 55.99. Found [**1** + H]$^+$ 272.0916; $C_{15}H_{14}NO_4$ requires [**1** + H]$^+$ 272.0917. (Figures S1 a and b, and S2, Supplementary Material).

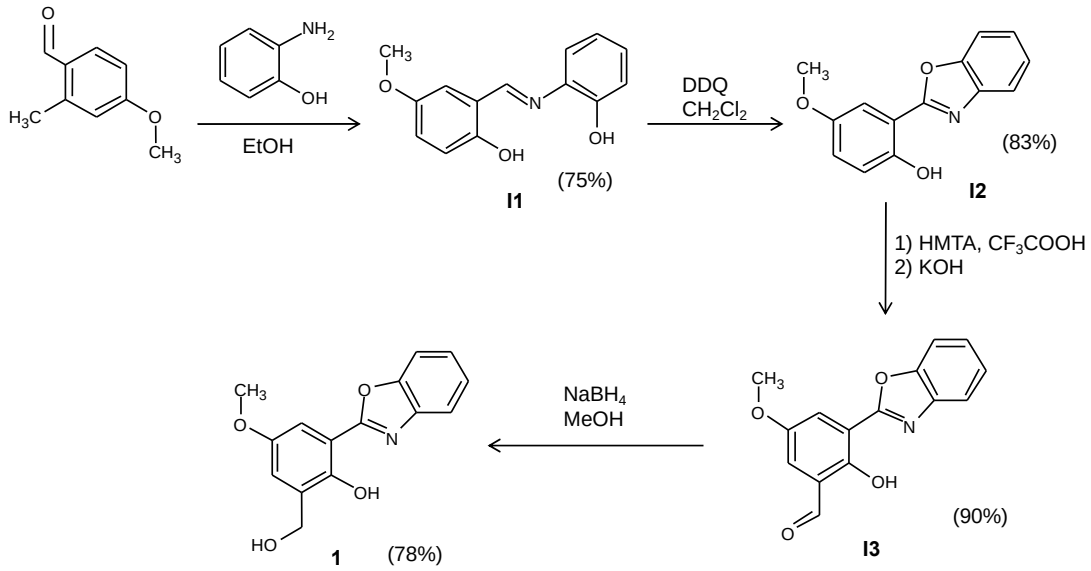

Scheme 1. Synthetic steps for **I1**-**I3** and **1**.

2-(2-hydroxy-3-hydroxyiminomethyl-5-methylphenyl)-benzimidazole **(2)**: In a 25 mL round-bottom flask, **I5** (252 mg, 1 mmol) was dissolved in 10 mL of EtOH at 50 °C. Separately, (NH_3OH)Cl (83.4 mg, 1.2 mmol) was dissolved in 4 mL of EtOH with subsequent addition of an aqueous solution of CH_3COONa (123.1 mg, 1.5 mmol). The later solution was added to the former one and the reaction mixture was left stirring for 16 h at reflux conditions. Afterwards, the solution was concentrated, and cooled until 0 °C to allow a fluffy greenish powder to precipitate. It was then collected, washed with

cold EtOH and hexane, and dried under reduced pressure to obtain 411 mg of **2** (Yield: 65 %). ^{1}H-NMR (DMSO-d_6, 300 MHz): δ (ppm) 13.66 (1H, s, Hb), 13.30 (1H, s, Ha), 11.30 (1H, s, Hc), 8.42 (1H, s, H12), 7.93 (1H, s, H8), 7.72 (1H, d, J = 6.82), 7.61 (1H, d), 7.59 (1H, s, H7), 7.30 (2H, br m, H4 and H5), 2.35 (3H, s, H10). ^{13}C-NMR (DMSO-d_6, 75 MHz): δ (ppm) 154.01, 151.38, 143.49, 140.63, 133.09, 127.82, 127.69, 127.48, 123.46, 122.53, 120.47, 117.94, 112.86, 111.60, 20.25. Found [**2** + H]$^{+}$ 268.1093; $C_{15}H_{13}N_3O_2$ requires [**2** + H]$^{+}$ 268.1086. (Figures S1 c and d, and S3, Supplementary Material).

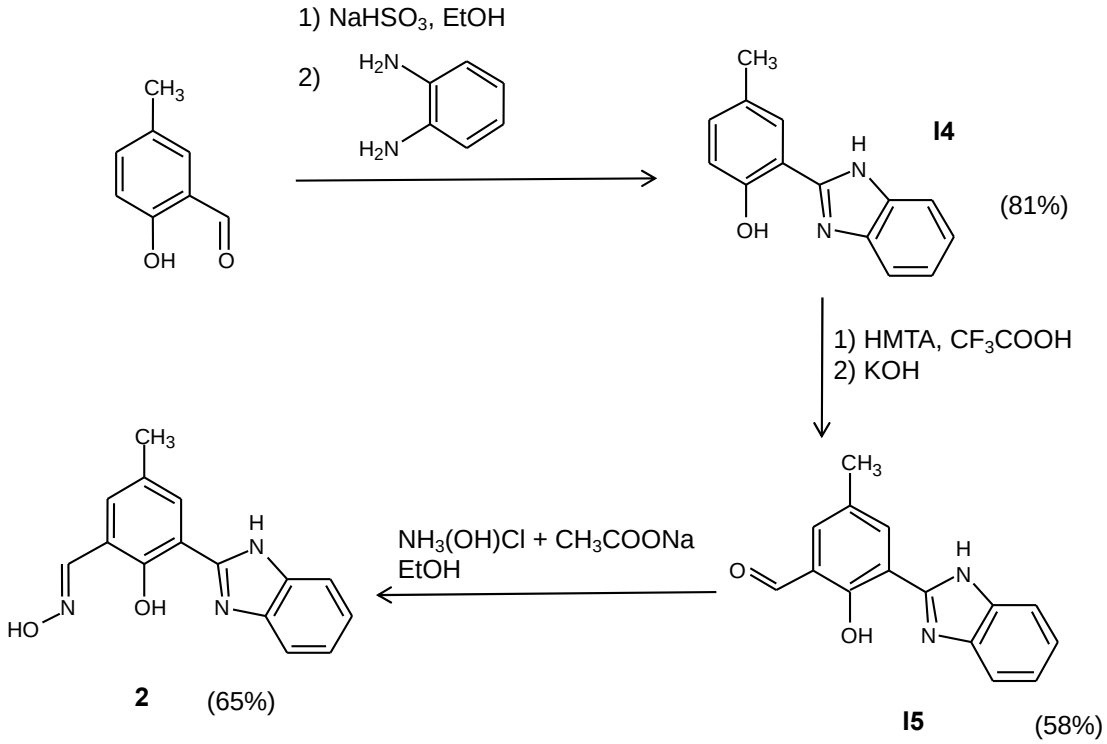

Scheme 2. Synthetic steps for **I4**, **I5**, and **2**.

X-ray crystal structure determination

Crystals of **2** suitable for X-ray diffraction were obtained by slow evaporation of an ethanolic solution. A crystal was mounted on a Stoe Stadivari diffractometer and was kept at 150 K during data collection. Using Olex2 [36], the structure was solved with the

SHELXT [37] structure solution program using Intrinsic Phasing and refined with the SHELXL [38] refinement package using Least Squares minimization. Graphical representation of the molecule was made with Mercury [36] and rendered with POV-ray [39]. The CCDC number is 2262555.

3. Results and Discussion

3.1. Synthesis and structural properties.

Compound **1** was designed in order to benefit from ESIPT known to occur in such 2-(2-hydroxyphenyl)benzoxazole derivatives [40] for probing the presence of metal ions in an aqueous medium. The feasibility of this process has recently been shown [30,31,40]. A methoxy group was introduced in **1** in place of the hydroxymethyl group reported previously in order to tune the ESIPT properties of the molecule and to evaluate its effect on the selectivity towards metal cations. The synthetic scheme for **1** is depicted on Scheme 1. Compound **1** was obtained in four steps from the commercial 2-hydroxy 5-methoxybenzaldehyde and 2-aminophenol. Compound **2** comprises a benzimidazole moiety coupled to a hydroxybenzene unit that bears an oxime group. The benzimidazole unit was chosen as it can act as a multifunctional detection unit serving as a fluorophore, it can coordinate metal ions, and it can allow ESIPT thanks to the *N* atom of the 5-membered ring that can bind the phenolic proton. The oxime group has been described to interact with hypochlorite ions [32,41-47], and can also permit a proton transfer from the hydroxy group by protonation of the *N* atom, thus also favoring ESIPT. Finally, with the OH from the oxime group being at the ortho position of the Schiff base, **2** shows a predefined cavity well-suited for the complexation of the Al^{3+} ion [48-50].

The synthetic procedure for obtaining **2** is shown on Scheme 2. Compound **2** was obtained in 4 steps from commercial 2-hydroxy-5-methylbenzaldehyde. The synthetic procedures for the intermediates are detailed in the Supplementary Material.

Crystals of **2** suitable for X-ray diffraction were obtained by slow evaporation of an ethanolic solution. The structure of **2** is shown on Figure 1. The unit cell contains an additional molecule of ethanol. Two internal hydrogen bonds take place. The phenolic and benzimidazolic protons are forming intramolecular hydrogen bonds with the *N* atom of the oxime group and the O atom of the phenol group, respectively. The distances are 1.912 Å and 2.132 Å for the OH(phenol)···*N*(oxime) and *N*(benzimidazole)H···O(phenol) hydrogen bonds, respectively, while the values of the O(phenol)H*N*(oxime) and *N*(benzimidazole)HO(phenol) angles are 147.04 and 120.73°, respectively. These values reveal that these hydrogen bonds are relatively strong, especially that formed between the phenolic H atom and the *N* atom of the oxime group. Moreover, a third hydrogen bond occurring between the O atom of the oxime group and the ethanol molecule is observed.

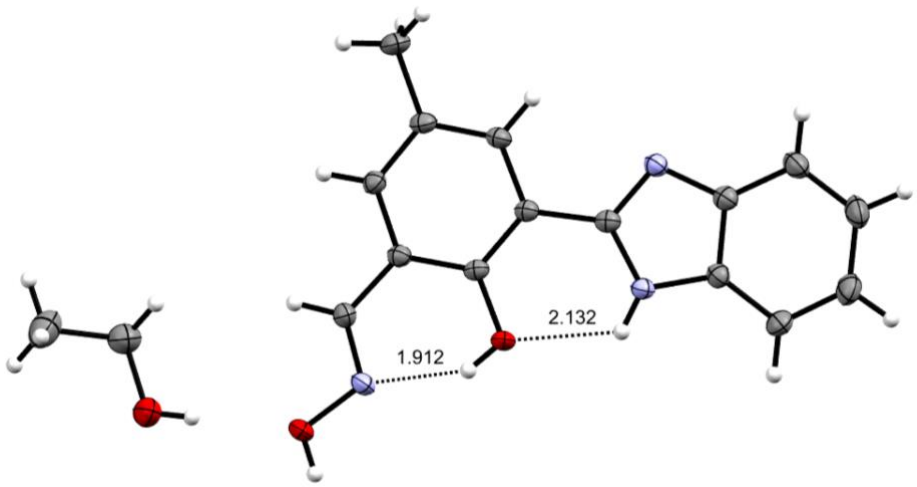

Figure 1. X-ray crystal structure of **2**·EtOH showing hydrogen bonds (dashed lines, values are given in Å). Color code: grey: carbon, red: oxygen, white: hydrogen, mallow: nitrogen.

3.2. Steady state spectral studies

The photophysical properties of **1** were investigated in 80 % aqueous EtOH. They are reported in Figure 3, left. The absorption spectrum of **1** shows a broad band with a maximum at 346 nm (corresponding to a molar absorption coefficient of 8000 L mol^{-1} cm^{-1}) and a structured band centered at 289 nm (absorption coefficient of 12 000 L mol^{-1} cm^{-1}). The low energy band can be assigned to the coupling of the OH group of the phenol with the *N(*oxazole) atom, whereas the high energy band is due to the absorption of the chromophore without coupling [51]. A weak tail that extends up to 500 nm could be a consequence of Mie Scattering observed for organic chromophores in water [52].

Excitation of **1** at 340 nm resulted in three emission bands. The highest energy band (386 nm), being relatively sharp, is attributed to Raman scattering of the solvent. The band observed at 405 nm can be assigned to the emission of the enol form, while the broad red-shifted band centered at 496 nm is attributed to the emission of the keto form, a consequence of the ESIPT process (Figure 2). Although ESIPT active probes generally show damping of the ESIPT efficiency in aqueous medium, the intensity of the keto form is here still relatively important with respect to that of the enol form. This could be due to either aggregation of **1** in water or to a water-assisted enhancement of the ESIPT process [53-54].

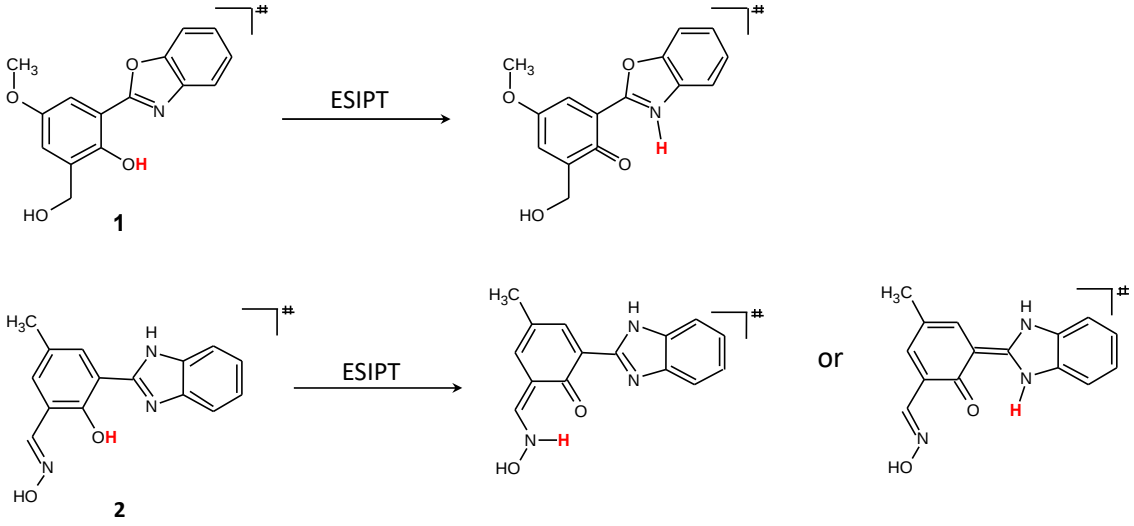

Figure 2. Representation of the ESIPT process prone to occur in **1** and **2**.

The fact that ESIPT occurring in **1** is strictly an excited state phenomenon can be emphasized by the very close similarity of the excitation and absorption spectra, ensuring that both emission bands originate from the same species in the ground state [55].

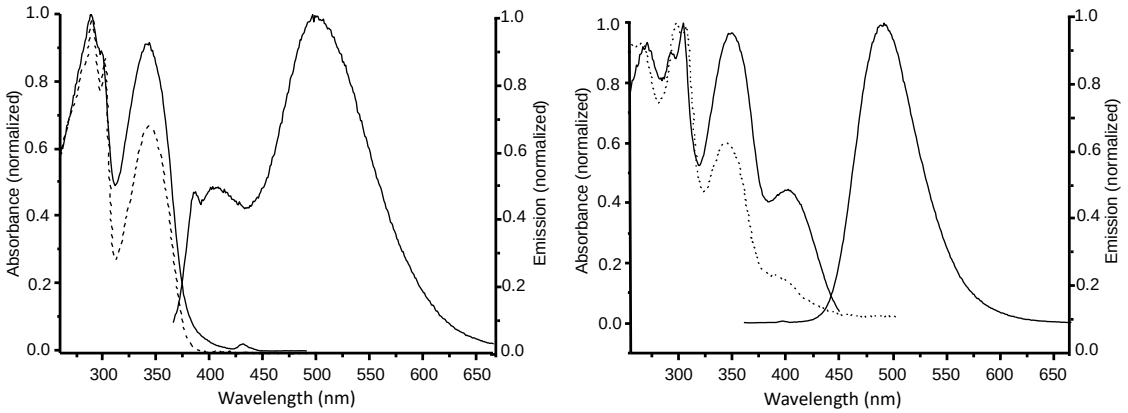

Figure 3. Left: normalized absorption (dashed trace), emission (λ_{exc} = 340 nm) and excitation spectra (λ_{em} = 503 nm) of **1** (EtOH:H_2O 1:4, 15 μM); right: normalized

absorption (dashed trace), emission (λ_{exc} = 349 nm) and excitation spectra (λ_{em} = 490 nm) of **2** (THF:H_2O 0.5:99.5, 15 μM).

The quantum yield of **1** was measured relatively to norhamane (2.1%) and quinine sulfate (2.2 %). These values are very close, showing the reliability of the measurements. An average value of 2% was then deduced, taking into account the emission of both the enol and keto forms. This value is moderate, showing that **1** is not a highly emissive compound.

The photophysical properties of **2** were investigated in 99.5% aqueous THF (Figure 3, right). A 15 μM solution of **2** shows absorption bands with maxima at 380, 344, 307, 296, and 264 nm, with absorption coefficients of 1 333, 5 333, 8667, 9334, and 8667 L mol^{-1} cm^{-1}, respectively. Based on descriptions of other hydroxyphenyl-benzimidazole derivatives, the lower energy bands are due to a π-π* transition assigned to the closed conformer or enol form of the ligand. The band at 344 nm is expected to be due to π-π* transitions of the open solvated conformer [51-56]. Finally, the band at 380 nm is thought to correspond to the phenolate anion that may have formed in solution and is in equilibrium with the protonated form [57 - 58]. The presence of this band shows that the phenolic proton is highly acidic. The tail that extends to the visible part of the spectrum could also be a consequence of Mie Scattering [52].

Excitation of **2** at 349 nm mainly resulted in a broad emission band centered at 490 nm. The high Stokes shift of this band is consistent with the keto emission of the molecule, a consequence of the ESIPT mechanism (schematized in Figure 2). Interestingly, the enol emission of the ligand appears at 365 nm with an extremely low intensity (Figure S4, Supplementary Material).

In the case of **2** also, the intensity of emission of the keto form is important relatively to that of the enol. As evidenced by the crystal structure of **2,** two relatively strong intramolecular hydrogen bonds take place. This, combined with the fact that the acidity of the phenolic protons increases in the excited state [58], has the effect of redistributing the electronic density around the oxygen atom, thus also enhancing the acidity of the phenolic proton by weakening the phenol O-H bond, and then possibly facilitating the proton transfer. Besides, there are other possible explanations to this keto-predominant emission. It could be due to either aggregation of the molecules in water or to a water-assisted enhancement of the ESIPT process, as previously described [53, 54]. Also, it has been reported that electron-donating substituents of the phenol part of a hydroxy-benzimidazole molecule were lowering the acidity of the proton of the OH group, thus decreasing the rate of the ESIPT process and promoting the enol emission [60]. It can therefore be anticipated that electron-withdrawing substituents linked to the hydroxybenzene group, such as the oxime group and the benzimidazole moiety, have the opposite effect, resulting in an increase of the acidity of the phenolic proton, thus promoting the keto emission. This points to the fact that the enol to keto phototautomerization is greatly favored in **2**, thus the emission corresponds almost exclusively to that of the keto tautomer. To complete the analysis of the ESIPT mechanism for Compound **2**, it is important to note that this mechanism can produce *a priori* two different keto forms. For both of them, the proton is transferred from the O-H group of the phenol moiety, but the receiving atom could be either the nitrogen of the benzimidazole moiety or the nitrogen of the oxime group, as presented in Figure 2. Based on the results of the crystal structure of this compound (Figure 1), which shows a preformed intramolecular hydrogen bond between the hydrogen of the phenol group and the nitrogen of the oxime entity, it can be postulated that the preferential proton transfer

occurs in this direction. Finally, the quantum yield of **2** was measured with 9,10-diphenylanthracene and quinine sulfate as references, giving values of 12.9 % and 12.1%, respectively. Thus, an average value of 12.5% was deduced from these measurements. This value is one order of magnitude higher than that determined for **1**.

3.3. Sensing capabilities of 1 and 2

Sensitivity investigations

Sensing studies of **1** were performed in a EtOH:H_2O 1:4 medium. The aptitude of **1** to interact with cations was investigated by fluorescence. Results are shown on Figure 4, left. Either no change or a slight change in the emission spectrum of **1** was observed in presence of an excess (5.3eqs) of the Cd^{2+}, Hg^{2+}, Mg^{2+}, and Fe^{2+} ions. A quenching of 30, 80, and almost 100% of the intensity of the keto band was observed upon addition of Ni^{2+}, Fe^{3+}, and Cu^{2+}, respectively. More remarkably, an increase in emission intensity of 140% and 270% associated to a blue shift of 15 nm and 45 nm was observed with the Zn^{2+} and Al^{3+} ions, respectively.

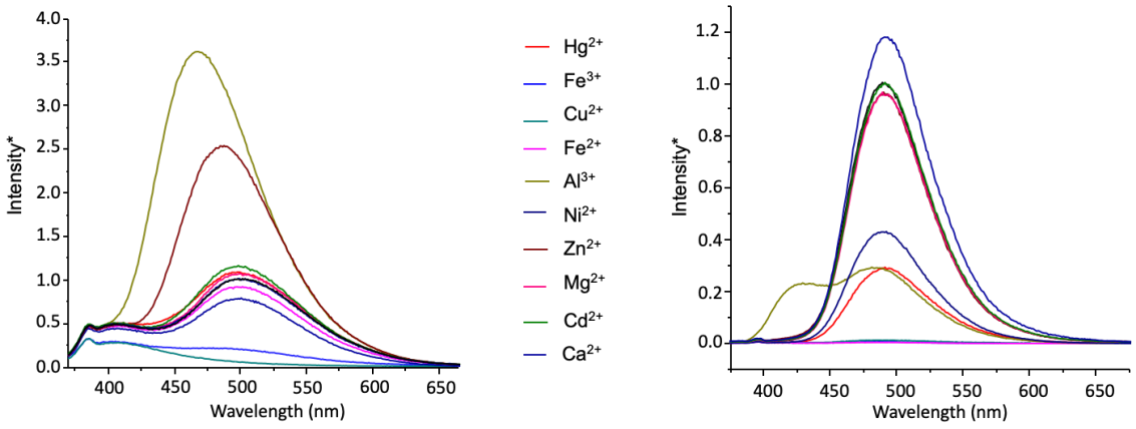

Figure 4. Left: emission spectrum of **1** in presence of 5.3eqs of cations (λ_{exc} = 340 nm, 14.7 µM, EtOH:H_2O 1:4); right: emission spectrum of **2** in presence of 5.3eqs of different cations (λ_{exc} = 349 nm, 18.7 µM, 99.5% aqueous THF). The color code used for each

cation is the same for both compounds and is shown in middle of the figure. *The emission intensity was normalized to that of **1** and **2**, respectively.

The limit of detection (LOD) of **1** was found to be ~3 µM and ~ 0.3 µM for Zn^{2+} and Al^{3+}, respectively (see Supplementary Material, Figures S5 and S6) [61]. The value found for Al^{3+} corresponds to a LOD of 0.008 ppm, two orders of magnitude below the maximum limit of 0.2 ppm allowed in drink water.

The sensing properties of **2** which shows a highest emission efficiency than **1**, and, thus, potentially, a better sensitivity, were similarly investigated. The emission spectrum of **2** upon addition of the same metal ions than tested for **1** is reported on Figure 3, right. The Mg^{2+} and Cd^{2+} ions have almost no impact on the emission of **2**, while 5.3eqs of the Ni^{2+} and Hg^{2+} ions resulted in a decrease of 57% and 70% of the emission of **2**, respectively, without noticeable shift. The presence of Cu^{2+}, Fe^{2+} and Fe^{3+} almost totally quenched the emission of **2**. Finally, addition of Al^{3+} resulted in a new band centered at 427 nm with an intensity 70% lower than that of **2**.

As **2** was designed to potentially interact with hypochlorite ions, the emission spectrum was recorded upon addition of a solution of sodium hypochlorite. It is shown on Figure 5, as well as that in presence of other anions. A dramatic decrease in intensity of the band centered at 490 nm and a low-intense blue-shifted band showing a maximum at 455 nm was observed. The latter was only observed in the presence of the ClO^- anions, showing selectivity for this ion. Interestingly, *N*-(phosphonomethyl)glycine, an herbicide widely used and also known as glyphosate, induces a decrease of 75% of the initial intensity of **2**, while its main metabolite, aminomethylphosphonic acid (AMPA), leads to a decrease of 40% of the initial intensity. This shows that **2** could also be a candidate to probe the presence of these species.

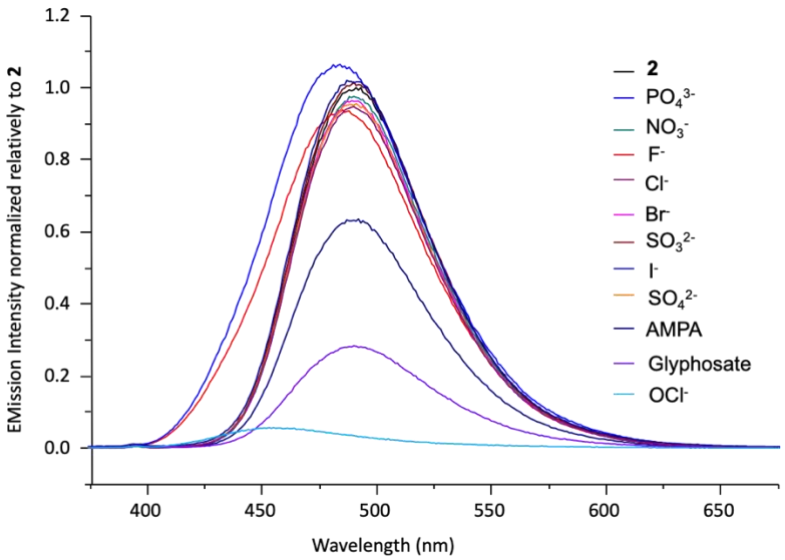

Figure 5. Emission spectrum of **2** (λ_{exc} = 349 nm, 18.7 μM, 99.5% aqueous THF) in presence of 5.3eqs of anions.

Upon evaluating the LODs of **2** towards Al^{3+} and ClO^-, a linear ratiometric response was found for Al^{3+} in the range of 1.5-28.4 μM with a LOD of 0.14 μM, corresponding to 3.7 ppb (Figure S7, Supplementary Material). In the case of the hypochlorite ion, the emission titration could not be used to calculate the LOD because the emission band of **2** and the band observed in presence of ClO^- overlap. The absorption titration was then used. A linear ratiometric response of **2** against this species in the range 5 μM-30 μM was found with a LOD of 1.12 μM. (Figure S8, Supplementary Material).

Sensing mechanism

Investigations were further conducted in order to get a better understanding on the sensing mechanism of **1** and **2** towards the Al^{3+} and ClO^- ions and to have a deeper insight on the

probe/species interaction with respect to the chemical nature of **1** and **2**. Indeed, it has been found that the response of **1** and **2** towards Al^{3+} was a ratiometric one. The mass spectrum of the aluminum complex of **1** shows a peak value at *m/z* 567.1349 (Figure S9, Supplementary Material), corresponding to the complex formula $[2(\mathbf{1}\text{-}H)^{-}+Al^{3+}]^{+}$. The m/z value evidences the loss of the phenolic proton in the Al complex and is the reason why ESIPT cannot exist anymore in presence of the Al^{3+} ion, thus leading to a decrease of the band corresponding to the keto emission and enhancing the band of the complex of phenolate species. The remaining emission due to the keto form testifies to the presence of some remaining free **1**. Similarly, the signal at 13.64 ppm on the ^{1}H NMR spectrum of the Al complex formed with **2** corresponding to that of the phenol group disappears along with that of the benzimidazole *N-H* group (13.28 ppm). Further, the signal corresponding to the C=N-O-*H* oxime group (11.27 ppm) undergoes a slight downfield shift to 11.51 ppm, with an important loss in intensity until almost completely disappearing while a new peak appears next to the one assigned to the N=C-*H* proton of the oxime moiety (8.40 ppm). These two observations tend to show that the oxime group also actively takes part in the recognition event between **2** and Al^{3+}. The ESI-MS spectrum of the Al complex (Figure S10, Supplementary Material) reveals the presence of a mono-charged species that corresponds to the formula $[\mathbf{2}\text{-}2H+Al^{\mathbf{3+}}]^{+}$. This result confirms the formation of the complex and suggests *i)* the loss of two protons and *ii)* a **2**:Al stoichiometry of 1:1. The apparent loss of a third proton indicated by the NMR experiment is thought to be due to an exchange with a labile proton from water used to solubilize the metal salt. These results confirm that ESIPT in **2** is inhibited in presence of Al^{3+}, explaining the quenching of the emission band at 490 nm and the enhancement of the band at 427 nm, which is assigned to the aluminum complex of the deprotonated ligand.

The Job's method of continuous variations was then used to verify the complexation ratio between **2** and Al^{3+} in a DMSO:H_2O 1:9 solution to eliminate the distortions originated from the Mie Scattering effect. The result shown on Figure 6 confirms a 1 to 1 stoichiometry.

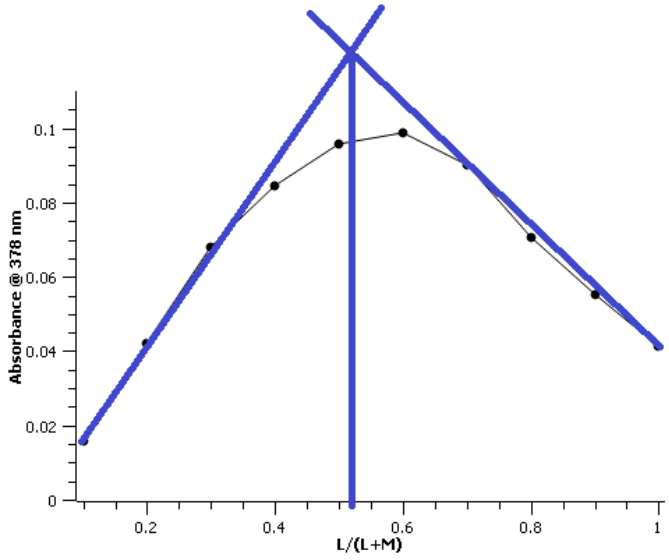

Figure 6. Job Plot for $[Al(\mathbf{2})]^+$. Total concentration = 16.9 μmol/L, L and M represent the ligand and metal concentration, respectively.

While it has been reported that the Job's method is outdated and provides results with low confidence for supramolecular host-guest systems, it is still valid for the study of inorganic complexes [29]. The 1:1 stoichiometric ratio for the Al complex of **2**, also allows the use of the Benesi-Hildebrand equation to calculate the binding constant of this interaction. A value of 1.42 x 10^6 M^{-1} was found (Figure S11, Supplementary Material). Typical binding constant range lies between 3.31 x 10^4 M^{-1} and 2 x 10^7 M^{-1} for probes that have a similar structure than **2** [28,31], showing that the value obtained for $[Al(\mathbf{2})]^+$ sits well in the upper part of that range.

It has been described that the C=N bond can be either cleaved by ClO^- to form an aldehyde [41,42,47], or transformed into a nitrile oxide [43]. Figure 7 shows how the ^{1}H NMR spectrum of **2** evolves with time after addition of 1eq of ClO^-. The signals of the benzimidazole N*H* and phenol O*H* protons immediately coalescence and merge into a broad signal, while that of the oxime N-O*H* group broadens. However, neither the signal that would be due to an aldehyde group is observable, nor the loss of the *H*-C=N proton that corresponds to the nitrile oxide entity is seen. To further verify the fact that the aldehyde corresponding to deoximation is not formed, **I5**, the compound analogous to **2**, but bearing an aldehyde group, was synthesized. The signal of the C(O)*H* proton appeared at 10.47 ppm (Figure S12, Supplementary Material). Comparison of the emission spectrum of this aldehyde with both that of **2** and **2** in presence of ClO^- (Figure S13, Supplementary Material) allows to unambiguously conclude that deoximation of **2** does not happen upon exposure to a hypochlorite solution for a few minutes. Indeed, the emission spectrum of the solution containing the aldehyde compound is red-shifted (maximum at 525 nm) with respect to that of **2**, while the presence of ClO^- results in a blue-shifted emission (maximum at 454 nm). The red shift observed for the aldehyde derivative was expected as a stronger donor-acceptor interaction occurs, the aldehyde group being more electron acceptor than the oxime [45]. The evolution with time of the ^{1}H NMR spectrum in presence of 1eq of ClO^- shows that, if the signal of the C=N-O-*H* proton first broadens, it then goes back to a sharper signal within 5 days. Meanwhile, the signals of the phenol and benzimidazole protons split into two broad signals. As the signal of the phenolic proton (13.2 ppm) is impacted upon addition of ClO^-, it is reasonable to believe that an interaction responsible of the inhibition of the ESIPT process described above occurs with the anion. Also, at day 5, signals corresponding to the formation of **I5** are observed at 10.49 and 8.21 ppm. The relative quantity of the aldehyde derivative is

9%, showing that deoximation has slowly occurred, and smoothly evolves to 14% at day 11. Note that upon heating the sample at 60°C over 3h did not lead to any aldehyde formation (Figure S14, Supplementary Material).

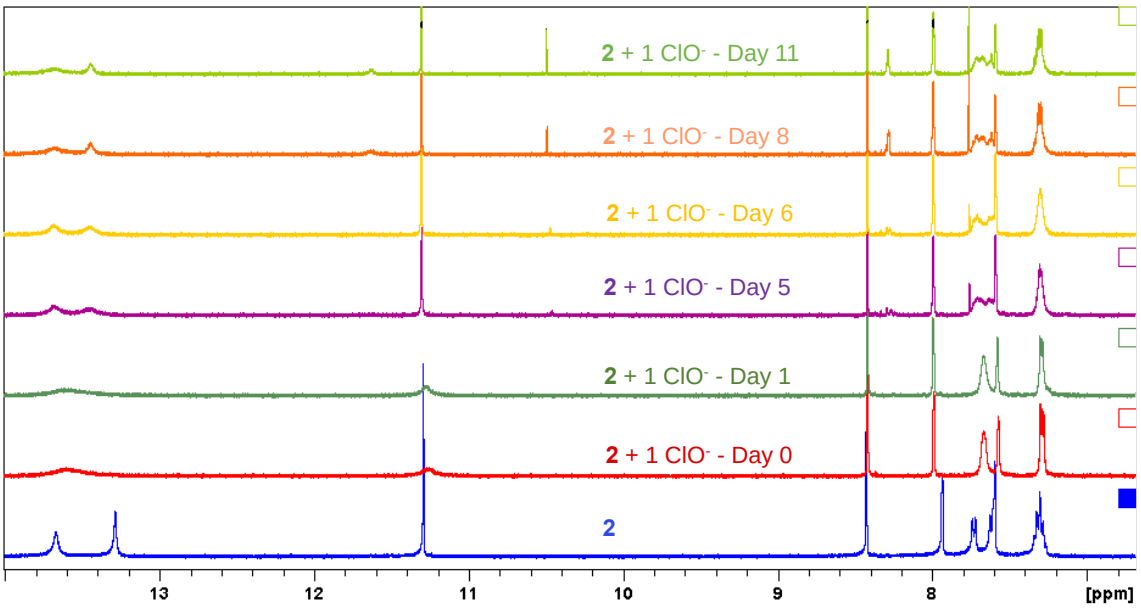

Figure 7. Evolution with time of the ^{1}H NMR spectrum of **2** in presence of 1eq ClO^-.

3.3. Influence of interferents

The foregoing studies have emphasized the fact that **1** and **2** could allow the detection of some anions and cations. In order to evaluate the selectivity with which this detection could be done, emission spectra were recorded in presence of interferents. The emission of **1** and **2** have shown to be strongly impacted by the Al^{3+} ion as a unique emission band appeared in both cases. Figure 8a compares the intensity of the emission band observed for free **1**, and upon successive addition of Al^{3+} and several cations. The presence of the Hg^{2+}, Ni^{2+}, Cd^{2+}, and Mg^{2+} ions does not hinder the detection of Al^{3+}, while the Zn^{2+}, Fe^{2+}, Fe^{3+}, and Cu^{2+} cations inhibits it. Similar results were obtained with **2** (Figure 8b),

with the difference that the emission of **2** in presence of Al^{3+} is almost not affected by the presence of Zn^{2+}.

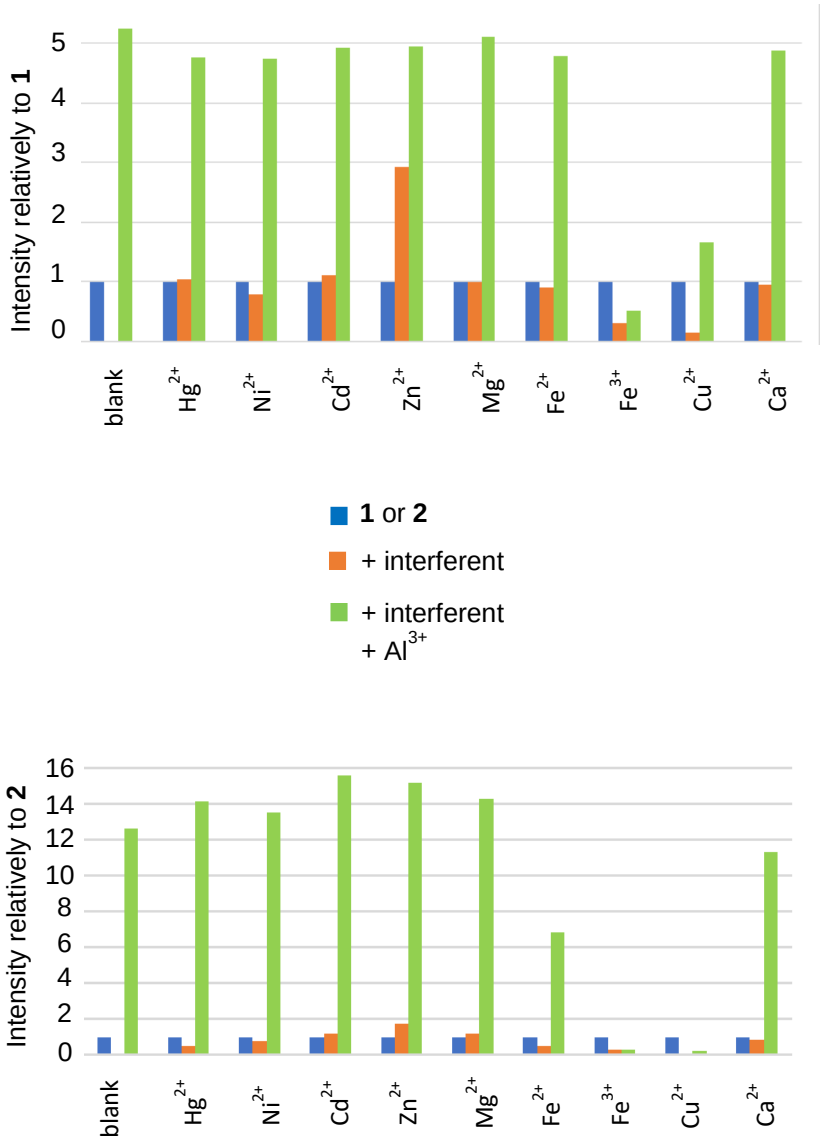

Figure 8. (a) Intensity of emission of **1** (λ_{exc} = 340 nm), and (b) intensity of emission of **2** in presence of another cation upon addition of Al^{3+} (λ_{exc} = 349 nm). Concentrations were **1**: 15 µM; **2**: 19 µM; metal cations: 80 µM. Solvent for **1** was EtOH:H_2O 1:4, and THF:H_2O 0.5:99.5 for **2**.

Finally, the influence of pH on the interaction of **2** with Al^{3+} was investigated (Figure 9). A basic medium (pH = 10) slightly quenches the 490 nm band (keto form). This result is consistent with the sensing mechanism described above: a basic medium facilitates deprotonation, making easier the inhibition of the ESIPT mechanism and promoting the complexation of the aluminum cation. On the other hand, an acidic medium induces a drop of both emission bands due to the quenching by H^+ ions [62]. Thus, the pH variation has no negative impact on the recognition of the Al^{3+} ion by **2**, despite a drop of sensitivity in acidic media. Finally, the emission of **2** in the pH range 1-14 has been recorded (Figure S15). Basically, emission of **2** is decreased upon decreasing pH from 7 to 1 without any noticeable shift in wavelength, while a drift to higher energies is observed when the pH is increased from 7 to 14. However, the band observed for basic values of pH is different from that observed in presence of Al^{3+}. Indeed, the most important blue shift is observed for the most basic solutions (maximum of emission at 450 nm for a pH of 13). This band is different both in shape and intensity from that observed in presence of Al^{3+}, reinforcing the interest of using **2** as an Al^{3+} probe. Moreover, considering that the addition of the Al^{3+} cation has the effect to slightly acidify the aqueous medium, it is clear that the emission response of **2** towards Al^{3+} is due to complexation and not because of a change in pH.

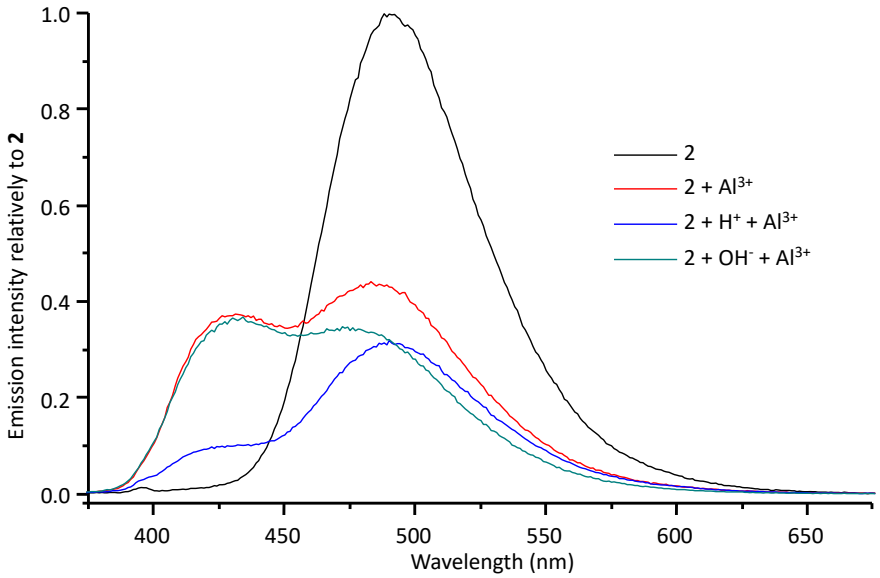

Figure 9. Emission spectrum of **2**, and **2** in presence of Al^{3+} upon addition of acidic (pH = 4) or basic (pH = 10) solutions. (λ_{exc} = 349 nm, 18.7 µM, 99.5% aqueous THF).

4. Conclusions

A benzoxazole derivate, **1**, and a benzimidazole derivative, **2**, were designed and synthesized in order to benefit from the ESIPT process in the optical sensing of cations. In the case of **2**, an oxime group was chosen to additionally interact with hypochlorite anions.

Their sensing properties were investigated in presence of a large amount of water, and even almost pure water in the case of **2**. Compound **1** is effective in the recognition of the Al^{3+}, Zn^{2+}, Fe^{2+}, and Cu^{2+} ions as its emission spectrum is dramatically impacted, while that of **2** is seriously impacted by the Al^{3+}, Ni^{2+}, Hg^{2+}, Fe^{2+}, and Cu^{2+} ions. More interestingly, selective optical sensors to Al^{3+} and ClO^- could be designed with **2** as a unique emission band is observed in each case. Only the Cu^{2+}, Fe^{2+} and Fe^{3+} ions could hinder the detection of Al^{3+} by almost totally quenching the overall emission. Compound

2, the most emissive one, has also shown a relative sensitivity to AMPA and glyphosate with a decrease in emission intensity of 40% and 75%, respectively, while no drastic change was observed with the other anionic species investigated.

Investigations on the sensing mechanism have shown that sensitivity to Al^{3+} was due to inhibition of the ESIPT process occurring in **1** and **2**. Also, even though the interaction between **2** and ClO^- is not fully understood, the fast recognition of the anion has been evidenced to occur through weak interactions instead of an irreversible deoximation as usually described in the literature. Note that deoximation was shown to occur very slowly ($\geq$ 5 days). This is promising in view of the development of a hypochlorite optical sensor with a fast response.

Conflicts of interest

There are no conflicts to declare.

Acknowledgements

We thank CNRS and Ecole Polytechnique for financial support. AB thanks the EU for a postdoctoral fellowship (Grant Agreement AMD-821036), SW thanks the China Scholarship Council (grant number 202006380011), and BA thanks LabEx CHARMMMAT (ANR-11- LABEX-0039) for a postdoc fellowship.

References

[1] N. E. W. Alstad, B. M. Kjelsberg, L. A. Vøllestad, E. Lydersen, A. B. S. Poléo, The significance of water ionic strength on aluminum toxicity in brown trout (Salmo trutta L.), Environ. Pollut. 2005; 133 : 333-342. https://doi.org/10.1016/j.envpol.2004.05.030

[2] M. I. S. Verissimo, J. A. B. P. Oliveira, M. T. S. R. Gomes, Leaching of aluminum from cooking pans and food containers, Sens. Actuators B: Chem. 2006; 118: 192–197. https://doi.org/10.1016/j.snb.2006.04.061

[3] R. J. P. Williams, Recent aspects of aluminum chemistry and biology: a survey, Coord. Chem. Rev. 2002; 228: 93-97. https://doi.org/10.1016/S0010-8545(02)00072-3

[4] R. A. Yokel, Aluminum chelation principles and recent advances, Coord. Chem. Rev. 2002; 228: 97–113. https://doi.org/10.1016/S0010-8545(02)00078-4

[5] E. Delhaize, P. R. Ryan, Aluminum toxicity and tolerance in plants, PlantPhysiol. 1995; 10: 315–321. https://doi.org/10.1104/pp.107.2.315

[6] D. L. Godbold, E. Fritz, A. Huttermann, Aluminum toxicity and forest decline, Proc. Natl. Acad. Sci. U. S. A. 1998; 85: 3888-3892. https://doi.org/10.1073/pnas.85.11.3888

[7] J. Tria, E. C. V. Butler, P. R. Haddad, A. R. Bowie, Determination of aluminum in natural water samples, Anal. Chim. Acta. 2007; 588: 153–165. https://doi.org/10.1016/j.aca.2007.02.048

[8] K. C. Snowden, R. C. Gardner, Five genes induced by aluminum in wheat (triticum aestivum L.) roots, PlantPhysiol. 1993; 103: 855-861. https://doi.org/10.1104/pp.103.3.855

[9] B. Ulrich, R. Mayer, P. K. Khanna, Chemical changes due to acid precipitation in a loess-derived soil in central Europe, Soil Science, 1980; 58: 193-199. https://doi.org/10.1097/00010694-198010000-00005

[10] J. Wang, Y. Pang, A simple sensitive ESIPT on-off fluorescent sensor for selective detection of Al^{3+} in water, RSC Adv. **2014;** 4**:** 5845-5848. https://doi.org/10.1039/C3RA47104G

[11] G. Berthon, Aluminum speciation in relation to aluminum bioavailability, metabolism and toxicity, Coord. Chem. Rev. 2002; 228: 319–341. https://doi.org/10.1016/S0010-8545(02)00021-8

[12] P. Nayak, Aluminum: impacts and disease, Environ. Res. 2002; 89: 101–115. https://doi.org/10.1006/enrs.2002.4352

[13] C. S. Cronan, W. J. Walker and P. R. Bloom, Predicting aqueous aluminum concentrations in natural waters, Nature, 1986; 324: 140–143. https://doi.org/10.1038/324140a0

[14] K. Boonkitpatarakul, J. Wang, N. Niamnont, B. Liu, L. McDonald, Y. Pang, M. Sukwattanasinitt, Novel Turn-On Fluorescent Sensors with Mega Stokes Shifts for Dual Detection of Al^{3+} and Zn^{2+}, ACS Sensors, 2016; 1: 144–150. https://doi.org/10.1021/acssensors.5b00136

[15] G. K. Walkup, S. C. Burdette, S. J. Lippard, R. Y. Tsien, A New Cell-Permeable Fluorescent Probe for Zn^{2+}, J. Am. Chem. Soc. 2000; 122: 5644–5645. https://doi.org/10.1021/ja000868p

[16] J. Bradfield, Plant Carbonic Anhydrase, Nature, 1947; 159: 467–468. https://doi.org/10.1038/159467a0

[17] F. M. Kahan, H. Kropp, J. G. Sundelof, J. Birnbaum, Thienamycin: development of imipenen-cilastatin, J. Antimicrob. Chemother. 1983; 12: 1–35. https://doi.org/10.1093/jac/12.suppl_D.1

[18] E. Callender, K. C. Rice, The Urban Environmental Gradient: Anthropogenic Influences on the Spatial and Temporal Distributions of Lead and Zinc in Sediments, Environ. Sci. Technol. 2000; 34: 232–238. https://doi.org/10.1021/es990380s

[19]. S.E. Hrudey, L.C. Backer, A.R. Humpage, S.W. Krasner, D.S. Michaud, L.E. Moore, P.C. Singer, B.D. Stanford, Evaluating evidence for association of human bladder

cancer with drinking-water chlorination disinfection by-products. J. Toxicol. Environ. Health B Crit. Rev. 2015; 18: 213–241. https://doi.org/10.1080/10937404.2015.1067661

[20] H. Feng, Y. Ruan, R. Wu, H. Zhang, P.K.S. Lam, Occurrence of disinfection by-products in sewage treatment plants and the marine environment in Hong Kong, Ecotoxicology Environmental Safety, 2019; 181: 404-411. https://doi.org/10.1016/j.ecoenv.2019.06.034

[21] N. Altunay, A. Elik, C. Bulutlu, R. Gürkan, Application of simple, fast and eco-friendly ultrasound-assisted-cloud point extraction for pre-concentration of zinc, nickel and cobalt from foods and vegetables prior to their flame atomic absorption spectrometric determinations, Int. J. Environ. Anal. Chem. 2018; 98: 655–675. https://doi.org/10.1080/03067319.2018.1487063

[22] E. G. C. Ergün, A. Kenar, Simultaneous determination of copper(II) and zinc(II) via simple acid-base titrimetry using glass pH electrode acid-base titrimetry using glass pH electrode, Turk. J. Chem., 2018; 42: 257–263. https://doi.org/10.3906/kim-1703-83

[23] N. Ozbek, S. Akman, Method development for the determination of calcium, copper, magnesium, manganese, iron, potassium, phosphorus and zinc in different types of breads by microwave induced plasma-atomic emission spectrometry, Food Chem., 2016; 200: 245–248. https://doi.org/10.1016/j.foodchem.2016.01.043

[24] U. Celik, J. Oehlenschläger, Determination of zinc and copper in fish samples collected from Northeast Atlantic by DPSAV, Food Chem., 2004; 87: 343–347. https://doi.org/10.1016/j.foodchem.2003.11.018

[25] M. H. Lee, J. S. Kim, J. L. Sessler, Small molecule-based ratiometric fluorescence probes for cations, anions, and biomolecules, Chem. Soc. Rev., 2015; 44: 4185–4191. https://doi.org/10.1039/C4CS00280F

[26] H. C. Joshi and L. Antonov, Excited-State Intramolecular Proton Transfer: A Short Introductory Review, Molecules, 2021; 26: 1475 -1492. https://doi.org/10.3390/molecules26051475

[27] C. Yuan, S. Li, Y. Wu, L. Lu, M. Zhu, Zn(II)-selective and sensitive fluorescent chemosensor based on steric constrains and inhibition of ESIPT, Sens. Actuators B: Chem., 2017; 242: 1035-1042. https://doi.org/10.1016/j.snb.2016.09.149

[28] Y. W. Choi, G. J. Park, Y. J. Na, H. Y. Jo, S. A. Lee, G. R. You, C. Kim, A single Schiff base molecule for recognizing multiple ions: A fluorescence sensor for Zn(II) and Al(III) and colorimetric sensor for Fe(II) and Fe(III), Sensors and Actuators B: Chemical, 2014; 194: 343 - 352. https://doi.org/10.1016/j.snb.2013.12.114

[29] D. Brynn Hibbert, P. Thodarson, The death of the Job Plot, transparency, open science and online tools, uncertainty estimation methods and other developments in supramolecular chemistry data analysis, Chem. Commun. 2016; 52: 12792. https://doi.org/10.1039/C6CC03888C

[30] Y. Shang, S. Zheng, M. Tsakama, M. Wang, W. Chen, A water-soluble, small molecular fluorescence probe based on 2-(2′-hydroxyphenyl) benzoxazole for Zn^{2+} in plants, Tetrahedron Lett., 2018; 59: 4003–4007. https://doi.org/10.1016/j.tetlet.2018.09.057

[31] X. L. Yue, Z. Q. Wang, C. R. Li and Z. Y. Yang, Naphthalene-derived Al^{3+}-selective fluorescent chemosensor based on PET and ESIPT in aqueous solution, Tetrahedron Lett., 2017; 58: 4532-4537. https://doi.org/10.1016/j.tetlet.2017.10.044

[32] L. Wu, Q. Yang, L. Liu, A.C. Sedgwick, A. J. Cresswell, S.D. Bull, C. Huang, T.D. James, ESIPT-based fluorescence probe for the rapid detection of hypochlorite ($HOCl/ClO^-$), Chem. Commun. 2018; 54: 8522-8525. https://doi.org/10.1039/C8CC03717E

[33] J. Chang, K. Zhao and S. Pan, Synthesis of 2-arylbenzoxazoles via DDQ promoted oxidative cyclization of phenolic Schiff bases - a solution-phase strategy for library synthesis, Tetrahedron Letters, 2002; 43: 951-954. https://doi.org/10.1016/S0040-4039(01)02302-4

[34] J. Li, A. Gong, G. Shi and C. Chai, A novel ratiometric flurescent probe for the selective determination of HClO based on the ESIPT mechanism and its application in real samples, RSC Advances, 2019; 9: 30943. https://doi.org/10.1039/C9RA04569D

[35] A. M. Brouwer, Standards for photoluminescence quantum yield measurements in solution (IUPAC Technical Report), Pure Appl. Chem. 2011; 83: 2213–2228. http://dx.doi.org/10.1351/PAC-REP-10-09-31

[36] O. V. Dolomanov, L. J. Bourhis, R. J. Gildea, J. A. K. Howard, H. Puschmann, OLEX2: A complete structure solution, refinement and analysis program, J. Appl. Cryst. 2009; 42: 339-341. https://doi.org/10.1107/S0021889808042726

[37] G.M. Sheldrick, SHELXT-Integrated Space-Group and Crystal-Structure Determination, Acta Cryst. 2015; A71: 3-8. https://doi.org/10.1107/S2053273314026370

[38] C.F. Macrae, I. Sovago, S.J. Cottrel, P.T.A. Galek, P. McCabe, E. Pidcok, M. Platings, G.P. Shields, J.S. Stevens, M. Towler, P.A. Wood, Mercury 4.0: form visualization to analysis, design and prediction, J. Appl. Cryst. 2020; 53: 226-235. https://doi.org/10.1107/S1600576719014092

[39] Persistence of vision Pty. Ltd. 2004.

[40] P. F. Dick, F. L. Coelho, F. S. Rodembusch, L. F. Campo, Amphiphilic ESIPT benzoxazole derivatives as prospective fluorescent membrane probes, Tetrahedron Lett. 2014; 55: 3024–3029. https://doi.org/10.1016/j.tetlet.2014.03.103

[41] B. Guo, H. Nie, W. Yang, Y. Tian, J. Jing, X. Zhang, A highly sensitive and rapidly responding fluorescent probe with a large Stokes shift for imaging intracellular

hypochlorite, Sensors and Actuators B: Chemical, 2016; 236: 465. https://doi.org/10.1016/j.snb.2016.06.004

[42] S. I. Reja, V. Bhalla, A. Sharma, G. Kaur, M. Kumar, A highly sensitive fluorescent probe for hypochlorite and its endogenous imaging in living cells, Chem. Commun. 2014; 50: 11911. https://doi.org/10.1039/C4CC05356G

[43] M. P. Algi, A fluorescent hypochlorite probe built on 1,10-phenantroline scaffold and its ion recognition features, J. Fluor. 2016; 26: 487-496. https://doi.org/10.1007/s10895-015-1734-7

[44] X. Xu, Y. Qian, A novel pyridyl triphenylamine-BODIPY aldoxime: Naked-eye visible and fluorometric chemodosimeter for hypochlorite, Spectrochimica Acta Part A: Molecular and Biomolecular Spectroscopy, 2017; 183: 356-361. https://doi.org/10.1016/j.saa.2017.04.043

[45] W. Lin, L. Long, B. Chen, W. Tan, A ratiometric fluorescent probe for hypochlorite based on a deoximation reaction, Chem. Eur. J. 2009; 15: 2305 – 2309. https://doi.org/10.1002/chem.200802054

[46] P. A. Kim, D. Choe, H. So, S. Park, B. Suh, S. Jeong, K.-T. Kim, C. Kim, R.G. Harrison, A selective fluorescence sensor for hypochlorite used for the detection of hypochlorite in zebrafish, Spectrochimica Acta Part A: Molecular and Biomolecular Spectroscopy, 2021; 261: 120059. https://doi.org/10.1016/j.saa.2021.120059

[47] C. Wu, X. Lin, Q. Wang, Determination of hypochlorite via fluorescence change from blue to green based on 4-(1H-imidazo [4,5-f] [1,10]-phenantrolin-2-yl) benzaldehyde oxime, J. Fluor. 2021; 31: 1125-1132. https://doi.org/10.1007/s10895-021-02740-1

[48] P. Roy, Recent advances in the development of fluorescent chemosensors for Al(III), Dalton Trans., 2021; 50: 7156. https://doi.org/10.1039/D1DT00901J

[49] H. Kuzhandaivel, S. Banu Basha, I. D. Charles, N. Raju, U. Singaravelu, K. S. Nallathambi, Performance of 2-hydroxy-1-naphthaldehyde-2-amino thiazole as a highly selective turn-on fluorescent chemosensor for Al(III) ions. Detection and biological applications, J. Fluor. 2021; 31: 1041-1053. https://doi.org/10.1007/s10895-021-02722-3

[50] Y.-G. Zhang, Z.-H. Shi, L.-Z. Yang, X.-L. Tang, Y.-Q. An, Z.-H. Ju, W.-S. Liu, A facile fluorecent probe based on coumarin derived Schiff base for Al(III) in aqueous media, Inorg. Chem. Commun. 2014; 39: 86-89. https://doi.org/10.1016/j.inoche.2013.10.035

[51] P. Majumdar, J. Zhao, 2-(2-hydroxyphenyl)-benzothiazole (HBT)-rhodamine dyad: Acid-switchable absorption and fluorescence excited-state intramolecular proton transfer (ESIPT), J. Physical Chem. B, 2015; 119: 2384-2394. https://doi.org/10.1021/jp5068507

[52] H. Auweter, H. Haberkorn, W. Heckmann, D. Horn, E. Luddecke, J. Rieger, H. Weiss, Supramolecular Structure of Precipitated Nanosize β-Carotene Particles, Angew. Chem., Int. Ed. 1999; 38: 2188–2191. https://doi.org/10.1002/(SICI)1521-3773(19990802)38:15<2188::AID-ANIE2188>3.0.CO;2-%23

[53] A. Bhattacharyya, N. Guchhait, Exciplex formation between a pair of synthesized AIEgens leads to white light generation: a spectroscopic exploration, New J. Chem. 2020; 44: 10671–10680. https://doi.org/10.1039/D0NJ02489A

[54] L. McDonald, J. Wang, N. Alexander, H. Li, T. Liu, Y. Pang, Origin of Water-Induced Fluorescence Turn-On from a Schiff Base Compound: AIE or H-Bonding Promoted ESIPT?, J. Phys. Chem. B, 2016; 120: 766–772. https://doi.org/10.1021/acs.jpcb.5b10909

[55] Y.-P. Tong, S.-L. Zheng, X.-M. Chen, Structures, photoluminescence and Theorettcal studies of two Zn(II) complexes with substituted 2-(2-hydroxyphenyl)benzimidazoles, Eur. J. Inorg. Chem., 2005; 18: 3734-3741. https://doi.org/10.1002/ejic.200500174

[56] A. Bhattacharyya, S. Kumar Mandal, N. Guchhait, Imine-amine tautomerism vs. Keto-enol tautomerisation: Acceptor basicity dominates over acceptor electronegativity in ESIPT process through six-member intramolecular H-bonded network, J. Phys. Chem. A, 2019; 123: 10246-10253. https://doi.org/10.1021/acs.jpca.9b08646

[57] M. M. Henary, C. J. Fahrni, Excited state intramolecular proton transfer and metal ion complexation of 2-(2'-hydroxyphenyl)benzazoles in aqueous solution, J. Phys. Chem. 2002; 106: 5210-5220. https://doi.org/10.1021/jp014634j

[58] A. C. Sedgwick, L. Wu, H.-H. Han, S. D. Bull, X.-P. He, T. D. James, J. L. Sessler, B. Z. Tang, H. Tian, J. Yoon, Exited-state intramolecular proton-transfer (ESIPT) based fluorescence sensors and imaging agents, Chem. Soc. Rev. 2018; 47: 8842. https://doi.org/10.1039/C8CS00185E

[59] Q. Huang, Q. Guo, J. Lan and J. You, Tuning the dual emission of keto/enol forms of excited-state intramolecular proton transfer (ESIPT) emitters via intramolecular charge transfer (ICT), Dyes and Pigments, 2021; 193: 109497. https://doi.org/10.1016/j.dyepig.2021.109497

[60] N. Alarcos, M. Gutierrez, M. Liras, F. Sánchez, A. Douhal, An abnormally slow proton transfer reaction in a simple HBO derivative due to ultra fast intramolecular-charge transfer events, Phys. Chem. Chem. Phys. 2015; 17: 16257-16269. https://doi.org/10.1039/C5CP00577A

[61] IUPAC, Nomenclature, Symbols, Spectrochim. Acta Part B. 1978; 33: 241–245. https://doi.org/10.1016/0584-8547(78)80044-5

[62] S. Bhowal, A. Ghost, Highly selective fluorescent turn-on–off sensing of OH, Al^{3+} and Fe^{3+} ions by tuning ESIPT in metal organic frameworks and mitochondria targeted bio-imaging, RSC Adv. 2021; 11: 27787-27800. https://doi.org/10.1039/D1RA03078G